Journal of Marine Research, 52, 1037–1049, 1994

Currents under land-fast ice in the Canadian Arctic Archipelago Part 2: Vertical mixing

by R. F. Marsden[1], R. G. Ingram[2] and L. Legendre[3]

ABSTRACT

During an acoustic Doppler current profiler (ADCP) study of the velocity field under land-fast ice, coincident CTD casts showed three instances of pronounced instability in the water column, immediately above and below the pycnocline. In this paper we demonstrate that the density inversions are associated with the passage of high frequency linear internal waves and finite amplitude waves. Contours of ADCP acoustic return intensity display pronounced vertical eddy-like features which may indicate overturning. A Richardson number calculation showed that even the most highly stratified portion of the pycnocline had sufficient vertical velocity shear to promote dynamic instability. Finally, we calculate that the vertical nutrient flux, resulting from the high frequency internal wave field, could supply a significant portion of the ice-algae nutrient budget.

1. Introduction

During the spring bloom, ice algae constitute the largest photosynthetic biomass in ice-covered polar seas, forming dense mats in the bottom few centimeters of the ice and at the ice-water interface (Cota *et al.,* 1987; Legendre *et al.,* 1992a). Legendre *et al.* (1992b) estimated that approximately 25% of the annual primary production in the Arctic Ocean takes place within the sea ice. Not only are they important ecologically, being the only source of food at a critical time for many pelagic animals, they also contribute to the biological pumping of CO_2 from the atmosphere into deep waters through the export of carbon from the surface associated with ice melt, having possible significance for the global biogeochemical flux of carbon (Legendre *et al.,* 1992a). During the transition from winter darkness to summer light conditions, the algae are initially light limited, however, late in the season, they can be nutrient limited in either nitrogen (Maestrini *et al.,* 1986) or silicon (Gosselin *et al.,* 1990). An acoustic Doppler current profiler (ADCP) was deployed through land-fast ice in Resolute Passage, North-West Territories with the objective of measuring the three components of the under-ice velocity field as part of a joint Canada-Japan study to

1. Physics Department, Royal Roads Military College, FMO, Victoria, B.C., Canada, V0S 1B0.
2. Department of Atmospheric and Oceanic Sciences, McGill University, 805 Sherbrooke Street West, Montreal, Quebec, Canada, H3A 2K6.
3. Département de Biologie, Université Laval, Québec, Québec, Canada, G1K 7P4.

determine factors responsible for algae growth during the April–May 1992 bloom. One month of measurements were taken from which Marsden *et al.* (1994) (hereafter MPI), obtained unambiguous estimates of the vertical velocity field. Thirty-one high frequency (< 1 hour periods) events, of 2 to 12 hours duration, were detected and were classified as linear and finite amplitude internal waves.

At mid-latitudes, internal solitons have been found to induce mixing and to be important in nutrient budgets. Sandstrom and Elliott (1984) suggested that solitary waves could account for all mixing required to meet phytoplankton nutrient requirements for the Scotian Shelf. They state '... the nonlinear manifestations of the internal tide can account for a large fraction of the internal tide energy and are energetic enough to be probably the primary mixing mechanism in the shelf break zone, which is estimated to be 20–30 km wide inshore from the shelf edge.' Haury *et al.* (1979), using a 200 kHz acoustic backscattering system, detected overturning in internal lee waves generated off Stellwagen Bank in Massachusetts Bay. They proposed that the associated mixing may be important to the biology of the region in enriching the surface layer. Pingree *et al.* (1986) showed that internal tides generated at the Celtic Sea shelf break propagated both seaward and on to the shelf, mixing nutrients to the surface in their wake. Recently Bogucki and Garrett (1993) have proposed a simple instability model to explain the mechanics of the breaking and decay of Korteweg-deVries type internal solitons. Where internal and finite amplitude waves at mid-latitudes are often generated through interaction of tidal flow with bottom topography, MPI suggested that under-ice internal waves may also develop from interaction of tidal flow with irregularities at the ice-water interface, particularly evident at ice keels.

In this paper, evidence will be provided to indicate mixing associated with the passage of linear internal waves and linear finite amplitude waves based on three sets of observations. First, conductivity, temperature and depth (CTD) profiles taken simultaneously with the passage of the waves indicated a severe disruption of the density structure between the pycnocline and ice-water interface. Second, the associated acoustic backscatter amplitude showed closed vertical circulation cells immediately below the pycnocline which we will argue result from vertical mixing. Third, the Richardson number fell below the critical 0.25 value immediately above and below the pycnocline during the passage of the events suggesting that conditions were suitable for shear instabilities to occur. Dissipation and eddy diffusivity estimates indicated sufficient mixing to satisfy a significant portion of ice algal nutrient requirements.

The study location, equipment layout and justification of the vertical velocities is given in MPI. The present paper will be divided into the following sections. Section 2 will present evidence of mixing in three conductivity, temperature and depth (CTD) profiles as well as in the acoustic backscatter amplitude. In Section 3, we will use the ADCP velocities and density profiles to calculate contours of Richardson number

and demonstrate that conditions suitable for mixing existed during the passage of internal waves. Section 4 will contain a discussion and concluding remarks.

2. Density inversions

The density profile was sampled using a Seabird SBE19 CTD at approximately noon each day from 23 April to 4 May. Supplementary casts were taken at irregular intervals. The salinity cell was broken on 5 May and could not be replaced until 16 May when, as was noted in MPI, the density structure had changed markedly. We will focus on two casts, one sampled on 22 April and the other on 1 May, which were taken during or immediately after the passage of a linear internal wave field and finite amplitude wave field respectively. A third cast, on 4 May, was also taken during the passage of another finite amplitude wave train and since its results were nearly identical to those obtained on 1 May, these will not be presented explicitly in this paper. Figure 1a shows a sequence of density profiles taken on 25 and 26 Apr. The dot-dashed line, taken at 9:40 Central Standard Time 25 April, is typical of profiles sampled during periods when none of the oscillations described in MPI were detected. There is a slightly unstable region between the ice-water interface and 5 m depth with a strong pycnocline from 10 to 15 m. Below the pycnocline, the water column is nearly isopycnal to approximately 80 m. A profile sampled later in the day at 14:39 (solid line), has pronounced inversions from the ice-water interface to 10 m and from 19 to 21 m depth. The density found at 19 m, was neutrally stable at 60 m suggesting a possible 40 m eddy. A subsequent cast made on 26 Apr (dashed line), shows a return to a stable density profile. Figure 1b is a time series of the vertical velocity sampled at 13 m, for the internal wave field listed as event 4 in MPI. Note the distinct 4 hour modulation in the amplitude. The time of the cast having the near surface instability is indicated by the vertical line and is clearly associated with the passage of this event. Figures 2a and b show similar sequences for a train of finite amplitude waves recorded on 1 May. Profiles taken on 30 April and 2 May are typical of quiescent periods (i.e. when high frequency internal waves and finite amplitude waves were not observed). On 1 May, however, the pycnocline has been nearly destroyed and there is a marked density inversion above 8 m depth. Again there was unstable stratification immediately below the pycnocline, from 19 to 21 m depth, with the depth of equivalent neutral stability at 30 m. Figure 2b shows that the cast was taken less than 10 min after the passage of four large, distinct wavelets of the solitary wave field listed as event 13 in MPI.

There are a number of possible sources of the density inversions. First, they may reflect horizontal advection of pools of more dense water. These major disruptions were seen, however, *only* in profiles sampled coincident with the passage of internal/solitary wave events. If horizontal advection were the source of the disruption, one would expect to observe density inversions associated with tidal advection during quiescent periods which, never occurred. A second possibility is that the density

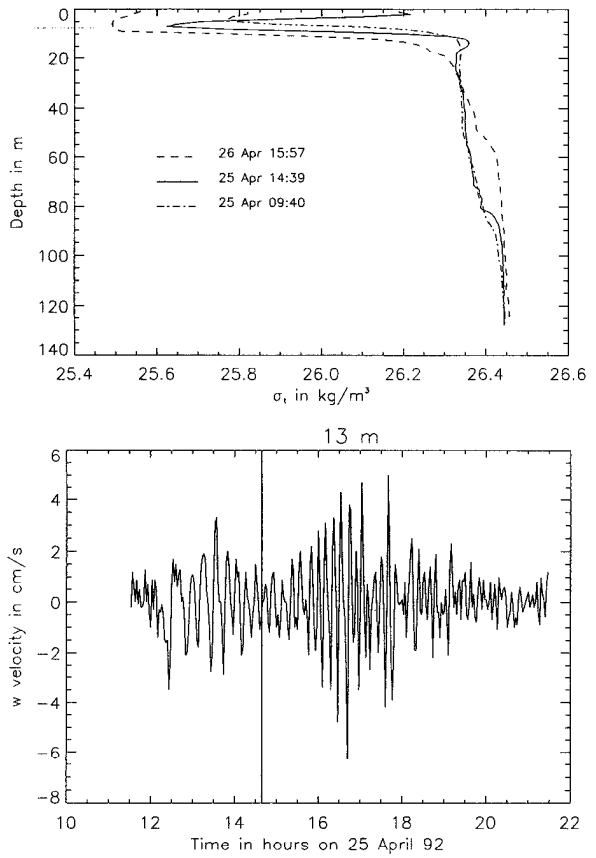

Figure 1. (a) Density profiles prior to, during (solid line) and after a high frequency wave event. (b) Vertical velocity recorded at 13 m with the time of the cast indicated by the vertical line.

inversions result from vertical advection cells established between the pycnocline and the ice-water interface. Figure 2b would argue against this since the density inversion occurs immediately *after* the passage of the last wavelet; there is no vertical velocity to advect the water parcel. The final possibility is that turbulence associated with the passage of the waves mixes the water column from pycnocline to the ice, which is the view that we favor. Note, however, that both options two and three offer a mechanism for the transport of nutrients from the pycnocline to the ice-water interface to supply the ice-algae.

Acoustic backscatter intensity. Flagg and Smith (1989) have proposed that ADCP return acoustic strength is proportional to the type and concentration of zooplankton scatterers in the water column. While their technique requires absolute calibration

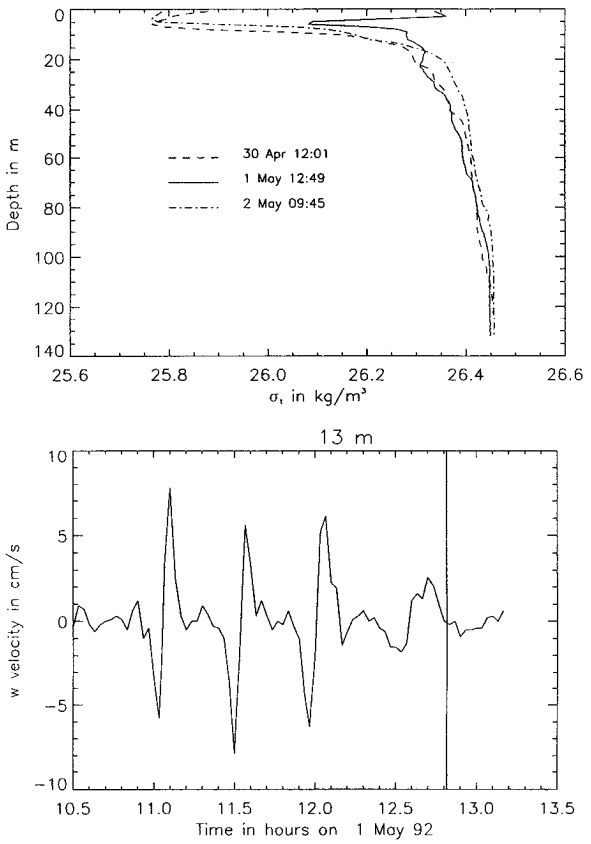

Figure 2. Same as Figure 1, for the finite amplitude wave detected on 1 May.

of each acoustic transducer, not performed in this experiment, Thomson *et al.* (1991) have shown that considerable information can be extracted from the relative return acoustic signal strength recorded in the average acoustic target strength (average AGC) for the four beams. The return target strength (TS) depends on the characteristics of the transducer, the scattering cross-section of the target, the distance from the target, and absorption in the water column given as

$$\frac{I_m}{I_a} = \frac{be^{-\alpha r}}{r^2} + A_n \tag{1}$$

where I_a is a reference intensity, I_m is the measured return intensity, b is the transducer gain, α is an attenuation coefficient, A_n is a noise term and $1/r^2$ represents expected geometric spreading along the (slanted) acoustic path. The ADCP records only the relative acoustic intensity given by the left hand side of (1) in decibels which,

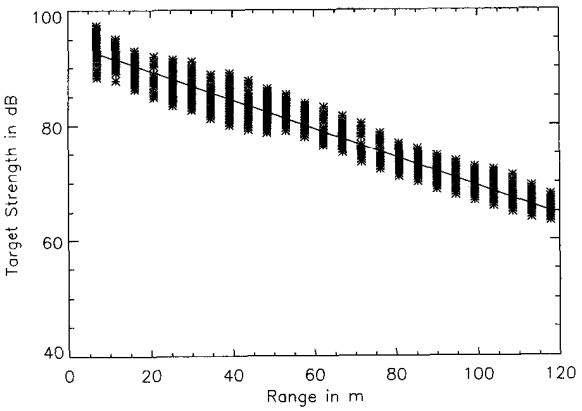

Figure 3. Target strength with the geometrical range correction incorporated ($TS + 20 \log r$) as a function of range for the return target strength of the event on 1 May. The slope of the line is the empirically determined attenuation coefficient.

ignoring a 1.5 dB error in the noise term, is given by

$$TS(r, t) = 10 \log \left(\frac{I_m}{I_a} \right) = 10(\log b - \alpha r - 2 \log r). \tag{2}$$

The dependence in $TS(r,t)$ is for each depth bin (r) and recorded ensemble (t). A mean target strength $\langle TS(r) \rangle$ was found by fitting (2), in a least squares sense, to the measured target strength $TS(r,t)$ for each event defined in MPI to determine $\log b$ and α. The anomaly $TS'(r,t) = TS(r,t) - \langle TS(r) \rangle$ represents a net fluctuation in acoustic return intensity as a function of time and depth over the event. Assuming that zooplankton act as passive scalars, the fluctuations can be interpreted as direct measurements of water parcel migration. Figure 3 shows the scatter of the fit for event 13 (1 May), indicating that the assumptions of inverse squared geometrical spreading and linear attenuation were appropriate.

Figures 4a and b are the contours of target strength anomalies corresponding to the events of Figures 1 and 2 respectively. CTD cast times are indicated by vertical lines in the plots. Undulations of the internal wave field in Figure 4a are clearly evident. For clarity, only data sampled within approximately 1.5 hours of the cast showing the near surface inversion are presented. Virtually every wave trough contains closed TS' contours with many having up to 3 dB anomalies from the event mean value, well above the noise level. Figure 4b shows similar contours for event 13 on 1 May with three of the four wavelets demarcated by particularly intense closed contours immediately below the pycnocline.

The closed contours could represent noise, mobility on the part of the zooplankton, or closed vertical circulation cells. The regularity and amplitude of the anomalies argue against random processes being responsible. Their regularity also suggests

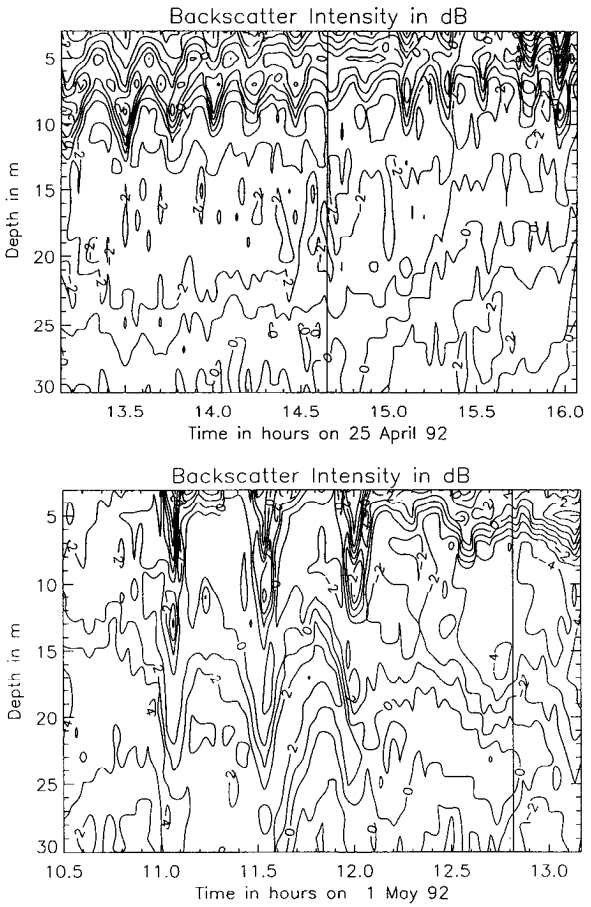

Figure 4. Contours of the anomaly of target strength return intensity for the event of (a) 25 April and (b) 1 May.

that zooplankton mobility is not responsible. Instances of patchiness should also appear outside the passages of the events, which were not observed. The most likely cause of the cells are advection by internal instability processes produced by the shears of the horizontal velocity field of the internal waves. Haury *et al.* (1979) show an acoustic picture taken by a 200 kHz echo sounder of two overturning events during internal wave generation in Massachusetts Bay. Their extrapolated temperature contours (their Fig. 3c) are closed cells, virtually identical to our closed acoustic anomaly intensity contours. Assuming that the closed cells are indicative of the movement of water parcels, we are unaware of any flow producing mechanically driven (as opposed to buoyancy driven) closed vertical circulation contours that does not also produce mixing.

3. Shear Instability

A well-known (LeBlond and Mysak, 1978), necessary condition for the generation of Kelvin-Helmholtz instabilities is that the Richardson number, defined as

$$Ri = \frac{-\frac{g}{\rho}\frac{\partial \rho}{\partial z}}{\left(\frac{\partial u}{\partial z}\right)^2 + \left(\frac{\partial v}{\partial z}\right)^2} = \frac{N^2}{\left(\frac{\partial u}{\partial z}\right)^2 + \left(\frac{\partial v}{\partial z}\right)^2} \tag{3}$$

be <0.25. Here, ρ is the water density, $\partial u/\partial z$ and $\partial v/\partial z$ are the vertical shears of horizontal velocity and N^2 is the Brunt-Vaisala frequency.

Ri was calculated for the two cases based on the two quiescent density profiles prior to the pronounced inversions. We wish to show where the shears associated with the internal events are strong enough to promote instability in the mean rather than the perturbed density profile. These estimates must be considered conservative since the internal wave field itself will deflect the isopycnals and decrease the stability, a condition not considered in this calculation. Furthermore, *Ri* calculated from the statically unstable profiles, taken during the passage of the waves, are not instructive as they indicate values <0.25 over virtually the entire top 20 m of the water column.

Figure 5a shows contours of *Ri* calculated for the 25 April event corresponding to the Figure 4a. Regions of $Ri < 0.25$ are shaded. *Ri* was continuously <0.25 below 15 m depth for the entire sampling period which corresponds to a region of extremely weak stratification shown in Figure 1a and numerous instances of closed acoustic backscatter intensities shown in Figure 4a. Above 10 m there are sporadic instances of subcritical values. Figure 5b shows the complete time series at 13 m depth of *Ri* calculated over the entire event. The critical 0.25 value is indicated by the solid horizontal line. The values are typically subcritical, however, there is a clear low frequency oscillation which corresponds exactly to the modulation in the amplitude of the vertical velocity shown in Figure 1b indicating that the variation of *Ri* has a strong tidal component due to stronger shears generated from either the background tidal flow or to high frequency perturbations of the wave field. Figure 6a shows contours of *Ri* for the 1 May event. Again there are many regions having subcritical values between 15 and 20 m, although not as extensive as for the 25 April event. There are three distinct times where subcritical values are seen above 15 m, corresponding to the passage of each wavelet as indicated in Figure 2b and 4b. Figure 6b shows *Ri* at 13 m depth as a function of time. Subcritical values occur at approximately 30 min intervals, coincident with the passage of each wavelet.

Cota *et al.* (1987) have proposed that, to within an order of magnitude, the ice algal nutrient demand in Lancaster Sound is 25 mmol m^{-2} over a 60 day period. Gargett

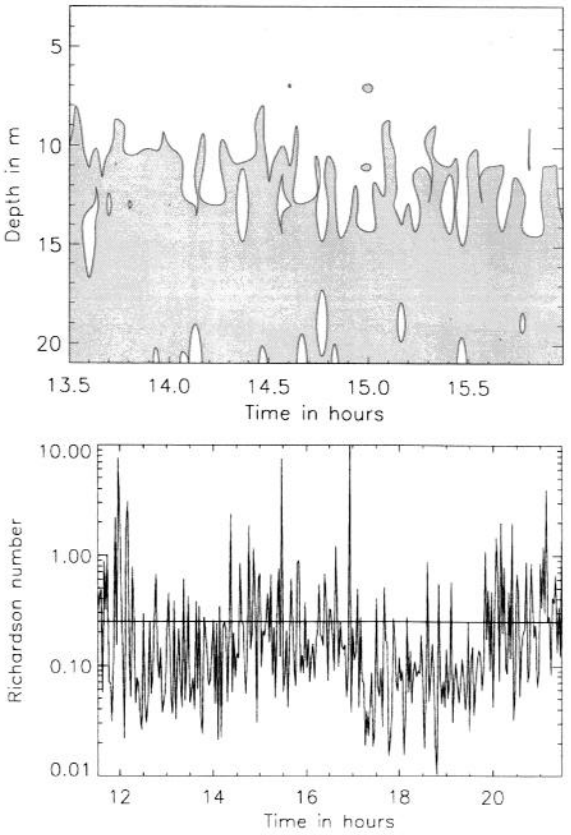

Figure 5. (a) Contours of Richardson number for the event of 1 May. (b) Time series of Richardson number at 13 m depth for the event of 1 May.

(1988) has shown that the turbulent dissipation rate ϵ correlates well with

$$"\epsilon" = \left| w' \, w' \frac{dw'}{dz} \right| \tag{4}$$

where w' is the fluctuating vertical velocity after the depth averaged mean was removed. Figure 7a shows a contour of "ϵ" as a function of depth and time for event 13 on 1 May and Figure 7b indicates the time series of "ϵ" for 13 m depth in the pycnocline. Maxima in dissipation occur during maxima in vertical velocity. An estimate (Osborn, 1980) for the vertical diffusion rate is

$$K = \frac{0.2\epsilon}{N^2} . \tag{5}$$

Assuming a typical value of N^2 of 7×10^{-5}rad ^{2} s^{-2} at 13 m depth and a vertical

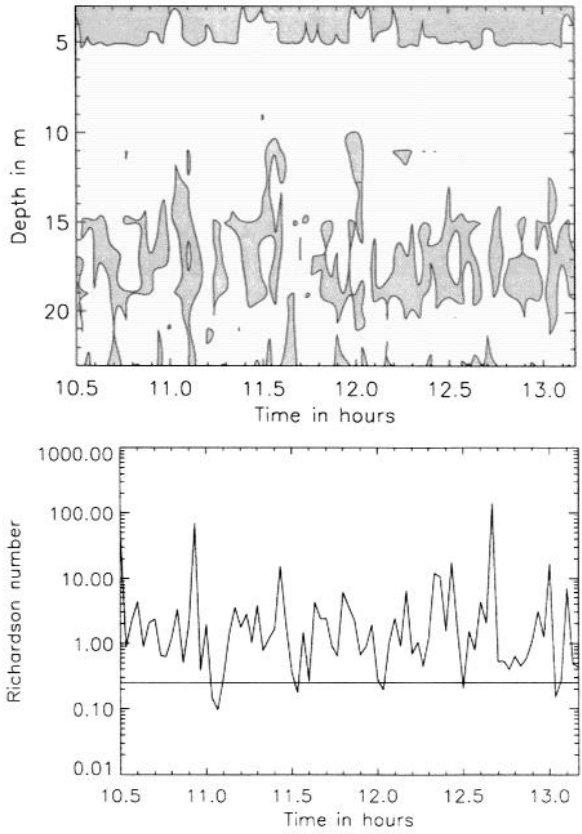

Figure 6. Same as Figure 5 for the event of 1 May.

nutrient gradient of 0.1 to 0.3 mmol m^{-4}, we calculate a nutrient supply of 1.5 mmol m^{-2} for the 19 events in the 13 day period from 22 Apr to 5 May with much higher values above and below the pycnocline. As shown in MPI, the surface pycnocline was not evident after 5 May, and our CTD casts indicated consistently unstable stratification at 13 m depth, during this period, preventing calculation of K. Assuming similarity to the 13 day measurement period, we estimate a minimum nutrient supply due to the high frequency events of about 6 mmol m^{-2} or 25% of the nutrient requirements suggested by Cota *et al.* (1987).

4. Discussion and conclusions

Evidence of vertical mixing associated with the passage of high frequency linear internal waves and finite amplitude waves described in MPI is presented. Three CTD profiles, of which we discuss two, taken simultaneously with the passage of the high frequency internal events showed pronounced inversions above and below the pycnocline. In all cases, the density profiles were relatively stable in preceding and

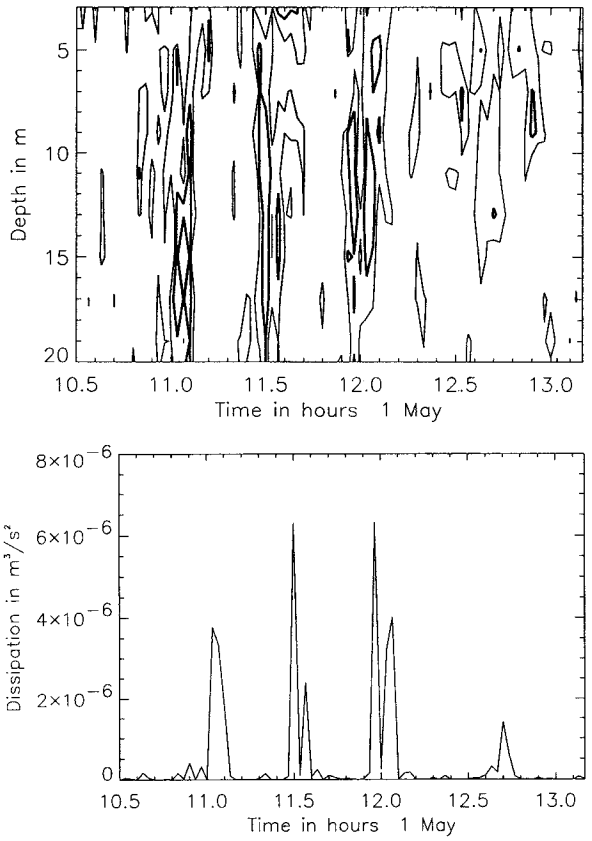

Figure 7. Contours (a) and time series at 13 m depth (b) of dissipation estimated by the Gargett (1988) technique for the event on 1 May 1992. Contours are 1.0×10^{-6} (thick line) and 1.0×10^{-7} $m^2 s^{-3}$ (thin line).

subsequent samples when evidence of the internal events was absent. Under the conservative assumption that the density profile was invariant to deflections from the wave field, the region immediately below the pycnocline had Richardson numbers less than 0.25. The pycnocline was situated at 13 m depth and was selected as giving the most pessimistic estimate of potential regions of dynamic instability and was examined in detail. The internal wave field indicated $Ri < 0.25$ during the entire passage of the event while the two finite amplitude wave cases indicated that Ri became critical during the passage of individual wavelets. Contours of anomalies of the return acoustic intensity showed numerous instances of closed contours which corresponded to the passage of the events and to subcritical Ri values in the pycnocline. Finally, an estimate of the eddy diffusivity indicated that a minimum of 25% of the nutrient demand of the ice-algae, proposed by Cota *et al.* (1987) could be provided by turbulence associated with the high frequency internal wave events.

Their nutrient demands are a spatial average applicable to the general Lancaster Sound, Barrow Strait region and are accurate only to an order of magnitude. Requirements in specific areas may vary markedly. Consequently, the fraction of the demand supplied by the high frequency internal wave field may be much larger than we cite.

Clearly, the evidence that we present is circumstantial. Our estimates of dissipation, based on the Gargett (1988) approach, are admittedly tenuous. It would have been preferable to have direct dissipation estimates during the passage of the internal waves which will be attempted in future studies. We have, however, confidence in the density gradients in the pycnoline and in the vertical shears. During quiescent periods (i.e. absence of high frequency waves), the background tidal velocity shears alone were not large enough to induce shear instabilities across the pycnocline, essential to promote mixing and the migration of nutrients from deep water to the ice-water interface. The only available mechanism is shear instability associated with the high frequency linear internal/finite amplitude wave fields.

Acknowledgments. We wish to thank Ann Gargett and Barbara-Ann Juszko for their suggestions on a early version of the manuscript.

REFERENCES

Bogucki, D. and C. J. R. Garrett. 1993. A simple model for the shear-induced decay of an internal solitary wave. J. Phys. Oceanogr., *23,* 1767–1776.

Cota, G. F., S. J. Prinsenberg, E. B. Bennett, J. W. Loder, M. R. Lewis, J. L. Anning, N. H. F. Watson and L. R. Harris. 1987. Nutrient fluxes during extended blooms of Arctic ice algae. J. Geophys. Res., *92,* 1951–1962.

Flagg, C. N. and S. L. Smith. 1989. On the use of the acoustic Doppler current profiler of measure zooplankton abundance. Deep-Sea Res., *36,* 455–479.

Gargett, A. E. 1988. A "Large-Eddy" approach to acoustic remote sensing of turbulent kinetic energy dissipation rate ϵ. Atmosphere-Ocean, *26,* 483–508.

Gosselin, M., L. Legendre, J. C. Therriault and S. Demers. 1990. Light and nutrient limitation of ice microalgae in Arctic waters. J. Phycol., *25,* 220–232.

Haury, L. R., M. B. Briscoe and M. H. Orr. 1979. Tidally generated internal wave packet in Massachusetts Bay. Nature, *278,* 312–317.

LeBlond, P. H. and L. A. Mysak. 1978. Waves in the Ocean. Elsevier, Amsterdam, 602 pp.

Legendre, L., S. F. Ackley, G. S. Dieckmann, B. Gullicksen, R. Horner, T. Hoshiai, I. A. Melnikov, W. S. Reeburgh, M. Spindler and C. W. Sullivan. 1992a. Ecology of sea ice biota. 2. Global significance. Polar Biol., *12,* 429–444.

Legendre, L., M. J. Martineau, J. C. Therriault and S. Demers. 1992b. Chlorophyll *a* biomass and growth of sea-ice microalgae along a salinity gradient (southeastern Hudson Bay, Canadian Arctic). Polar Biol., *12,* 445–453.

Maestrini, S. Y., M. Rochet, L. Legendre, and S. Demers. 1986. Nutrient limitation of the bottom-ice microalgal biomass. Limnol. Oceanogr., *31,* 969–974.

Marsden, R. F., J. R. Paquet and R. G. Ingram. 1994. Currents under land-fast ice in the Canadian Arctic Archipelago. Part 1: Vertical velocities. J. Mar. Res., *52,* 1017–1036.

Osborn, T. R. 1980. Estimates of the local rate of vertical diffusion from dissipation measurements. J. Phys. Oceanogr., *10,* 83–89.

Pingree, R. D., G. T. Mardell and A. L. New. 1986. Propagation of internal tides from the upper slopes of the Bay of Biscay. Nature, *321,* 154–158.

Sandstrom, H. and J. A. Elliott. 1984. Internal tide and solitons on the Scotian shelf: A nutrient pump at work. J. Geophys. Res., *89,* 6415–6426.

Thomson, R. E., R. L. Gordon and A. G. Dolling. 1991. An intense acoustic scattering layer at the top of a mid-ocean ridge hydorthermal plume. J. Geophys. Res., *96,* 4839–4844.

Received: *21 February, 1994;* revised: *17 May, 1994.*